Sublattice-ordered phases of Griffiths's three-component model

V. Talanquer and C. Varea
Facultad de Química, Universidad Nacional Autónoma de México, 04510 México, Distrito Federal, México

A. Robledo
Instituto de Física, Universidad Nacional Autónoma de México,
Apartado Postal 20-364, 01000 México, Distrito Federal, México
(Received 27 June 1988)

We describe the essential features of the mean-field phase diagram for the spin-1 Ising model with general nearest-neighbor interaction when sublattice ordering is made explicit. The phase diagram (in five-dimensional field space) can be classified into 84 zones where uniform with ordered phase coexistence is identified and multicritical behavior is determined. This generalized Ising model was studied extensively, in its ferromagnetic version, by Furman, Dattagupta, and Griffiths towards the end of the last decade. Here we complement that study with the antiferromagnetic phase behavior associated with the same model. Two different mappings between uniform and ordered phase existence conditions facilitated our task and indicated the interconnections that exist between ferromagnetic and antiferromagnetic properties in the model. Known features, like the "shield" region, appear reproduced in other energy-parameter locations, but also new features occur, such as additional tricritical and fourth-order critical lines connected by sixth-order critical points.

I. INTRODUCTION

In 1977 Furman, Dattagupta, and Griffiths (FDG) (Ref. 1) presented a comprehensive description of the global phase diagram associated with a model three-component system. This model can be thought of as the mean-field approximation to a spin-1 Ising magnet with the most general type of nearest-neighbor interactions, or, equivalently, to a fully packed alloy of three components with the same pair-interaction range. This, together with the work of Scott and van Konynenburg[2] on the closely related van der Waals model for a binary fluid mixture, allows for a thorough characterization of the unexpectedly rich phase behavior that these otherwise simple systems have. The FDG analysis was restricted, however, to the study of uniform phases, deliberately excluding the possibility of antiferromagnetism. In fact, only some discussions about the capabilities of the model for the description of crystallization phenomena by means of the study of its sublattice-ordered states have appeared since then in the literature,[3] and only a few specific system phase diagrams are known.[3] Nevertheless, it has been evident that the model must exhibit an abundant and possibly intricate phase equilibria involving sublattice-ordered phases.

For this reason, our main concern in this paper is the characterization of the prominent features of the phase diagrams of the FDG three-component model when sublattice ordering is considered. In particular, we work with two interpenetrating sublattices such that nearest-neighbor sites belong to different sublattices. For three-dimensional systems our analysis is directly applicable to simple-cubic and body-centered-cubic lattices. We refer briefly to the case when $k > 2$ interwoven sublattices are considered, and which are required, for example, in the study of the model when defined on a face-centered-cubic lattice[4] and also for some specific applications[5] on the simple-cubic lattice. The task of characterization of each kind of phase equilibria taking place under these circumstances (amongst ordered and also ordered and disordered states) is considerably simplified through the use of interconnections that occur between the ferromagnetic and the antiferromagnetic properties of the model.

The main tools in our analysis are two different equivalences that exist between sublattice ordered and disordered states. One of them relates properties of systems located in opposite energy triangles while the second one holds for systems located along the symmetric sections of the energy triangles. (In the work of FDG the eight octants spanned by the three interaction-energy parameters in the model are projected into eight "energy" triangles. The medians of these equilateral triangles constitute the symmetric sections. Definitions and notation, similar to those of Ref. 1, are explained in Sec. II.) These mappings allow us to use the known mean-field properties of the uniform, sublattice-disordered phases that characterize this model to delimitate the stability zones for the sublattice-ordered states. Also, they make possible the description of some important features of the antiferromagnetic phase equilibrium occurring in some locations of the global phase diagram in terms of known uniform (and, as we shall see, also ordered) phase equilibrium properties taking place somewhere else on the same diagram. The overall description of the phase diagram that we generate consists of a classification of the interaction-energy parameter space into 84 two-dimensional zones, with the property that within each region the corresponding system phase diagrams are topologically similar. Symmetry properties reduce the number of qualitatively different zones to 17 in which we identify the possible n-uniform and m-ordered-phase

coexistence together with their associated multicritical behavior.

In the ferromagnetic phase diagram,[1] multiplicity of phases and therefore the more complex system phase diagrams occur when all spin couplings are positive; this is the principal or P energy triangle. At the center of this triangle is located the so-called "shield" region where four-phase states occur and three lines of tricritical points originate. Towards the corners of this triangle there are other four-phase regions associated with three fourth-order critical points from which six additional lines of tricritical points extend beyond the P triangle.[1] Multiphase equilibria gradually simplify as the system is "taken away" from the P triangle and the interaction-energy parameters change signs. When all spin couplings are sufficiently negative, at the central region of the opposite S triangle, only single-phase states are found.[1] As expected, the opposite trend is true for sublattice-ordered phases. They are more numerous and phase equilibria are more complex when all couplings are antiferromagnetic, and these simplify and finally disappear as one moves to the fully ferromagnetic region of interaction energy space. In the central region of the S triangle we find three tricritical lines, associated with sublattice-ordered three-phase states, converging at a single sixth-order critical point. This antiferromagnetic region, that we refer to as the "rear-shield" region, has the features imagined by FDG as a possible alternative structure for the ferromagnetic shield region on the P triangle.[1] Because of the equivalence we have mentioned between sublattice-ordered and disordered states, the ferromagnetic features of system phase diagrams of some specific regions in interaction-energy space appear reproduced in other locations as antiferromagnetic properties, and vice versa for the antiferromagnetic features. Thus, the shield region of the P triangle is imaged three times into the adjacent Q triangles, and similarly, the rear-shield region of the S triangle appears again in the adjacent R triangles. The three ferromagnetic fourth-order critical points in the P triangle are found again as antiferromagnetic properties of the S triangle. In Sec. III we expand this outline of the global phase diagram.

The structure of the paper is as follows. In Sec. II we recall briefly the definition of the FDG model and describe the method developed to study its antiferromagnetic phases. To facilitate the description of our results we choose a notation close to that employed by FDG in their original paper, and therefore we delegate our compromise with the reader for clarity of presentation and physical information to a large extent to that excellent article. In Sec. III we present a description of the global phase diagram in terms of the locations, intersections, and nature of the tricritical and fourth-order critical lines which (together with the edges of the energy triangles) form the boundaries that separate different interaction-energy parameter zones. We also describe selected system phase diagrams representative of each zone. Again, as in Ref. 1, the phase diagrams we present employ only thermodynamic "field" or only thermodynamic "density" variables, and describe coexistence and critical manifolds or (hyper)surfaces with a notation that takes advantage of the permutation properties of the model variables. Section IV is a brief summary and discussion of results. In the following two papers we present applications to two different realizations of the three-component model, the first is to the case of binary alloys with one magnetic component and the second to a model of a solvent-amphiphile solution of the Wheeler-Widom type.[4] In both cases it is possible to appreciate the capability of the global phase diagram in providing complete descriptions.

II. THE THREE-COMPONENT MODEL AND ITS SUBLATTICE-ORDERED STATES

Consider a ternary mixture of N_x, N_y, and N_z particles of components X, Y, and Z, respectively, situated on the $N_x+N_y+N_z=N$ sites of a regular lattice. For uniform states the mean-field Helmholtz potential per site $\mathcal{f}'$, can be written as,

$$\mathcal{f}'=kT'(x\ln x+y\ln y+z\ln z)+q(a'yz+b'xz+c'xy)\ , \tag{1}$$

where k is Boltzmann's constant and T' the absolute temperature, q is the coordination number; a', b', and c', are phenomenological energy parameters, and x, y, and z represent the mole fractions of the three components. The close-packing condition

$$x+y+z=1 \tag{2}$$

implies infinite chemical potentials, but their differences are in general finite, of which two are independent. Therefore, the uniform equilibrium states occurring at temperature T' and chemical potential differences ν_1' and ν_2' are provided by points (x,y) in the triangle $1\geq x\geq 0$, $1\geq y\geq 0$, $1\geq x+y\geq 0$ that satisfy the equation

$$\Pi'(\nu_1',\nu_2')=\min_{x,y}\{(\mathcal{f}'-\nu_1'x-\nu_2'y)\}\ . \tag{3}$$

Equation (3) defines the (negative) of the pressure $-\Pi'$, i.e., the minimization determines x and y, and the resulting value is called Π'. The above condition leads to the relations

$$\nu_1'=kT'\ln(x/z)+q(b'z+c'y-a'y-b'x) \tag{4a}$$

and

$$\nu_2'=kT'\ln(y/z)+q(a'z+c'x-a'y-b'x)\ . \tag{4b}$$

Whenever Eq. (3) admits n minima of equal depth Π' at $(x_1,y_1),(x_2,y_2),\ldots,(x_n,y_n)$, we say that n phases coexist for the current values of the six thermodynamic "field" variables a', b', c', T', ν_1', and ν_2'. Since multiplication of Eq. (1) by a positive factor, that can be taken to be the inverse temperature $1/kT'$, does not affect phase coexistence, only five thermodynamic fields are relevant in the description of the FDG phase diagram. Also the adoption, as in Ref. 1, of the normalization condition

$$|a'|+|b'|+|c'|=1\ , \tag{5}$$

suggests the convenience of specification of two of the energy parameters in terms of the third. Choice of the tem-

perature scale is equivalent to giving a value to this third energy parameter. In the same spirit it is convenient to introduce[1] the "activity" variables

$$\zeta'_x=\exp(\nu'_x/kT')/\xi' , \tag{6a}$$

$$\zeta'_y=\exp(\nu'_y/kT')/\xi' , \tag{6b}$$

$$\zeta'_z=\exp(\nu'_z/kT')/\xi' , \tag{6c}$$

with

$$\xi'=\exp(\nu'_x/kT')+\exp(\nu'_y/kT')+\exp(\nu'_z/kT') , \tag{7}$$

and

$$\nu'_x=\nu'_1+\Pi', \quad \nu'_y=\nu'_2+\Pi', \quad \nu'_z=\Pi' . \tag{8}$$

In similarity with Eqs. (2) and (5) one has,

$$\zeta'_x+\zeta'_y+\zeta'_z=1 . \tag{9}$$

In their description of the global uniform-phase diagram, FDG employed the barycentric representation on equilateral triangles for the three sets of quantities, the energy parameters a,b,c, the activities ζ_x,ζ_y,ζ_z, and the mole fractions x,y,z. This consists in representing the point, say (a,b), with $|a|+|b|+|c|=1$ as the center of mass of three "masses" of magnitude a, b, and c, located at the vertices of an equilateral triangle. See Fig. 1. We indicate[1] with a capital letter the number of positive energy parameters, $P=3$, $Q=2$, $R=1$, and $S=0$. As shown in Fig. 2, there are one P and one S triangle and there are three Q and three R triangles. The subscripts in the notation in Fig. 2 are explained at the beginning of Sec. III. The symmetrical sections on these triangles are those for which the values of two of the energy parameters are equal. To every system, i.e., a and b fixed, there is a phase diagram to be described at each temperature in either an activity or a mole-fraction triangle. The barycentric representation exhibits an important symmetry property of the model: any permutation of a,b,c accompanied by the corresponding permutations of x,y,z and ζ_x,ζ_y,ζ_z leaves Eq. (1) unchanged and therefore indicates where any particular feature in the global phase diagram is reproduced. We employ below this particular set of coordinates in our description of diagrams with sublattice-ordered phases.

To study nonuniform ordered phases we now subdivide the lattice into two sublattices (α,β) such that $N/2$ points belong to each one, and the nearest neighbors of every site belong to the other sublattice. The mean-field Helmholtz potential per site is now written as

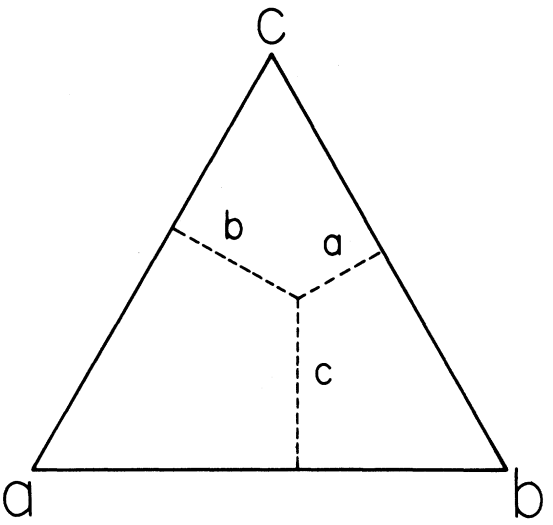

FIG. 1. Barycentric representation on equilateral triangles of the energy parameter space $0<|a|<1$, $0<|b|<1$, and $0<|c|<1$ with $|a|+|b|+|c|=1$.

$$\begin{aligned}\mathcal{f}=&(kT/2)(x^\alpha\ln x^\alpha+y^\alpha\ln y^\alpha+z^\alpha\ln z^\alpha\\&+x^\beta\ln x^\beta+y^\beta\ln y^\beta+z^\beta\ln z^\beta)\\&+(q/2)[a(y^\alpha z^\beta+y^\beta z^\alpha)+b(x^\alpha z^\beta+x^\beta z^\alpha)\\&+c(x^\alpha y^\beta+x^\beta y^\alpha)] ,\end{aligned} \tag{10}$$

where the unprimed $\mathcal{f}$, a, b, c, etc., variables help distinguish quantities referring to the sublattice divided system from those of the reference uniform system in Eq. (1). The superindexed x, y, and z indicate sublattice mole fractions. In parallel with Eqs. (1) and (4), the minimum condition,

$$\Pi(\nu_1,\nu_2)=\min_{x^\alpha,x^\beta;y^\alpha,y^\beta}\{\mathcal{f}-\tfrac{1}{2}[\nu_1(x^\alpha+x^\beta)+\nu_2(y^\alpha+y^\beta)]\} , \tag{11}$$

leads to the relations

$$\begin{aligned}\nu_1&=kT\ln(x^\alpha/z^\alpha)+q(bz^\beta+cy^\beta-ay^\beta-bx^\beta)\\&=kT\ln(x^\beta/z^\beta)+q(bz^\alpha+cy^\alpha-ay^\alpha-bx^\alpha) ,\end{aligned} \tag{12a}$$

and

$$\begin{aligned}\nu_2&=kT\ln(y^\alpha/z^\alpha)+q(az^\beta+cx^\beta-ay^\beta-bx^\beta)\\&=kT\ln(y^\beta/z^\beta)+q(az^\alpha+cx^\alpha-ay^\alpha-bx^\alpha) .\end{aligned} \tag{12b}$$

These expressions can be conveniently rewritten as

$$\begin{aligned}\nu_1-q[b(z^\alpha+z^\beta)+c(y^\alpha+y^\beta)-a(y^\alpha+y^\beta)-b(x^\alpha+x^\beta)]&=kT\ln(x^\alpha/z^\alpha)-q(bz^\alpha+cy^\alpha-ay^\alpha-bx^\alpha)\\&=kT\ln(x^\beta/z^\beta)-q(bz^\beta+cy^\beta-ay^\beta-bx^\beta)\end{aligned} \tag{13a}$$

and

$$\begin{aligned}\nu_2-q[a(z^\alpha+z^\beta)+c(x^\alpha+x^\beta)-a(y^\alpha+y^\beta)-b(x^\alpha+x^\beta)]&=kT\ln(y^\alpha/z^\alpha)-q(az^\alpha+cx^\alpha-ay^\alpha-bx^\alpha)\\&=kT\ln(y^\beta/z^\beta)-q(az^\beta+cx^\beta-ay^\beta-bx^\beta) .\end{aligned} \tag{13b}$$

Equations (13) show clearly that the transformation

$$T'=T,\quad a'=-a,\quad b'=-b,\quad c'=-c\ , \tag{14a}$$

$$\nu_1'=\nu_1-q[b(z^\alpha+z^\beta)+c(y^\alpha+y^\beta) -a(y^\alpha+y^\beta)-b(x^\alpha+x^\beta)]\ , \tag{14b}$$

and

$$\nu_2'=\nu_2-q[a(z^\alpha+z^\beta)+c(x^\alpha+x^\beta) -a(y^\alpha+y^\beta)-b(x^\alpha+x^\beta)]\ , \tag{14c}$$

implies that stable ordered states $(x^\alpha,x^\beta;y^\alpha,y^\beta)$ in the system a,b,c at temperature T and chemical potential differences given by ν_1 and ν_2 occur only if there are two solutions (x^α,y^α) and (x^β,y^β) of the uniform-phase equations (4) [with parameters defined through Eqs. (14)]. Similar equivalences hold between the occurrence of multiple (ordered or disordered) phases in the a,b,c systems and the number of distinct solutions of Eqs. (4). The stability of the ordered state $(x^\alpha,x^\beta;y^\alpha,y^\beta)$ is determined through the evaluation of the Hessian $\mathcal{H}$ of $\mathcal{f}$. Close to uniform states, $\mathcal{H}$ is conveniently written in terms of the variables,

$$x=x^\alpha+x^\beta,\quad y=y^\alpha+y^\beta,\quad \delta_x=x^\alpha-x^\beta,\quad \delta_y=y^\alpha-y^\beta\ , \tag{15}$$

since in that representation it has the form

$$\begin{vmatrix} \langle \mathcal{f}_{xx}\rangle & \langle \mathcal{f}_{xy}\rangle & \Delta\mathcal{f}_{xx} & \Delta\mathcal{f}_{xy} \\ \langle \mathcal{f}_{xy}\rangle & \langle \mathcal{f}_{yy}\rangle & \Delta\mathcal{f}_{xy} & \Delta\mathcal{f}_{yy} \\ \Delta f_{xx} & \Delta\mathcal{f}_{xy} & \langle \mathcal{f}'_{xx}\rangle & \langle \mathcal{f}'_{xy}\rangle \\ \Delta\mathcal{f}_{xy} & \Delta\mathcal{f}_{yy} & \langle \mathcal{f}'_{xy}\rangle & \langle \mathcal{f}'_{yy}\rangle \end{vmatrix}\ , \tag{16}$$

where $\langle \mathcal{f}_{ij}\rangle=\mathcal{f}_{ij}^{\alpha\alpha}+2\mathcal{f}_{ij}^{\alpha\beta}+\mathcal{f}_{ij}^{\beta\beta}$, $\Delta\mathcal{f}_{ij}=\mathcal{f}_{ij}^{\alpha\alpha}-\mathcal{f}_{ij}^{\beta\beta}$, and $\langle \mathcal{f}'_{ij}\rangle=\mathcal{f}_{ij}^{\alpha\alpha}-2\mathcal{f}_{ij}^{\alpha\beta}+\mathcal{f}_{ij}^{\beta\beta}$, with $\mathcal{f}_{ij}^{\alpha\beta}=(\delta\mathcal{f})/(\delta x_i^\alpha \delta x_j^\beta)$ $(x_1^\alpha=x^\alpha,\ x_2^\alpha=y^\alpha)$. The matrix associated with Eq. (16) is diagonalized by blocks at $\delta_x=\delta_y=0$. The zeros of the uppermost block represent the instabilities of uniform states against other uniform states, and are the usual spinodal lines of the ferromagnetic FDG model. The zeros of the bottom block represent the instabilities of uniform states against ordered states. The term with the minus sign in $\langle \mathcal{f}'_{ij}\rangle$ indicates that the spinodal lines resulting from the bottom block of $\mathcal{H}$ precisely correspond to the uniform-against-uniform state instabilities of the image system on triangle $a=-a'$, $b=-b'$, $c=-c'$.

To make use of the known uniform-phase FDG diagram in determining phase diagrams that allow for sublattice-ordered phases, we employ the above-described mapping between systems in opposite triangles a,b,c and $-a,-b,-c$ in the following way. For given values of a, b, and c (or T) we first determine the boundaries in

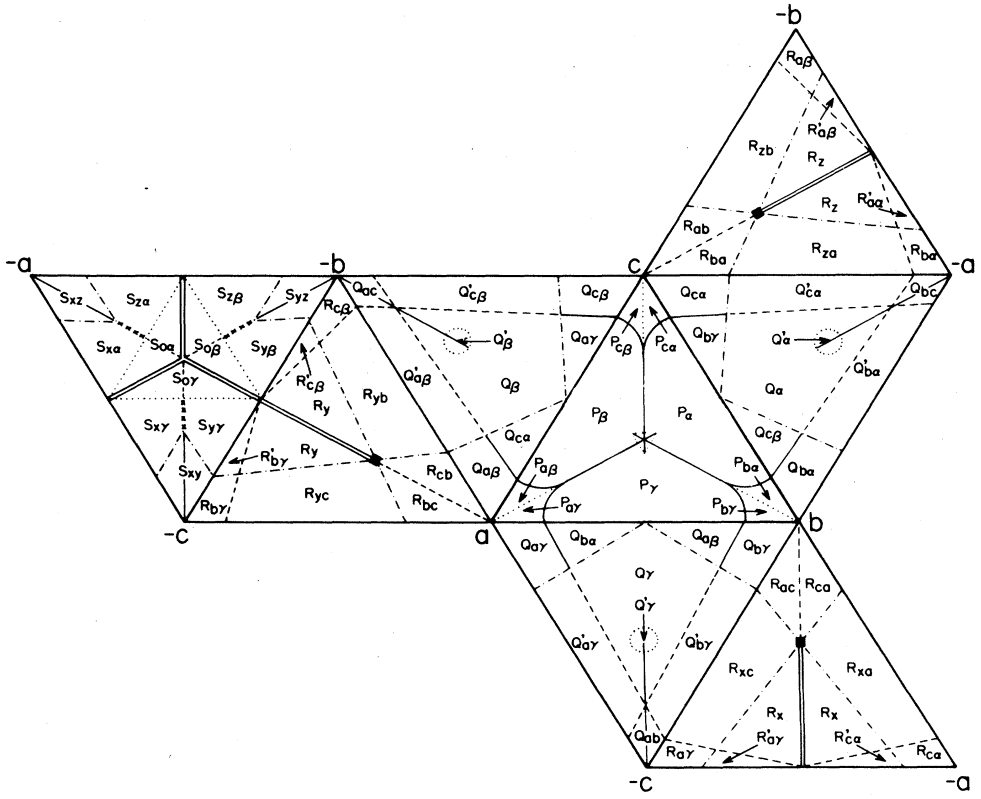

FIG. 2. Projection of the complete global phase diagram on the eight energy triangles. The capital letters that denote different phase diagram zones indicate the number of positive energy parameters a, b, and c; $P=3$, $Q=2$, $R=1$, and $S=0$. The subindexes help identify sets of equivalent regions. These are obtained by permutations of α,β,γ in the same manner as a,b,c. See the text for a more complete explanation of notation in this figure.

(ν_1,ν_2) space that delimit the zone or zones where stable (but possibly not all equilibrium) ordered states appear according to the transformation in Eqs. (14). Outside these regions there can only occur uniform states. In determining the boundaries in this space for stable ordered states, we find it useful to represent the uniform-phase diagrams (for systems with fixed interaction parameters a',b',c' and temperature T') in the field space (ν_1',ν_2'), where we indicate not only the loci of possible coexistence and associated critical points, but also the different uniform-phase stability zones. As shown in Fig. 3(a), two-phase coexistence is represented by a simple line, three-phase coexistence by the intersection of three two-phase coexistence lines, etc. The stability condition appears in this figure as a set of spinodal lines that delimit different stability regions, and, for our purposes, very conveniently, the superposition of spinodal regions that contain the coexistence lines, clearly correspond to those regions at which multiple solutions to Eqs. (4) are possible. Thus, the calculation of spinodal curves at a given temperature for a system described by the interaction parameters a', b', and c' defines, through Eqs. (14), those zones where a system characterized by the set $a=-a'$, $b=-b'$, and $c=-c'$ exhibits stable ordered states at the same temperature.

Inside the regions where ordered states occur in (ν_1,ν_2) space it is necessary to determine through direct calculations the coexistence and critical lines amongst the possible ordered phases as well as those between these ordered phases and the (known) uniform-phase equilibria within the region. Phase coexistence, between ordered, ordered and disordered, or disordered states requires, of course, the equality of the pressure $p=-\Pi$ in addition to that of T, ν_1, and ν_2. The expression for Π associated with the ordered state $(x^\alpha,y^\alpha;x^\beta,y^\beta)$ is

$$\Pi=\tfrac{1}{2}\{kT\ln(z^\alpha z^\beta)+q[(a+b-c)(x^\alpha y^\beta+x^\beta y^\alpha)+2ay^\alpha y^\beta+2bx^\alpha x^\beta]\}\ . \quad (17)$$

In Fig. 3(b) we show a typical phase diagram that results after such calculations are performed. The ordered states appearing in it correspond to those indicated by the spinodal regions in Fig. 3(a), the solid lines represent two-phase coexistence, dashed lines indicate second-order transitions, and their intersections (critical end points) bound different kinds of phase coexistence.

The approach we have just outlined can be generalized to investigate the model's phase equilibrium properties when the principal lattice has a different geometry or when it is subdivided in a different manner. Consider, for example, the case of k sublattices such that the nearest neighbors of every site in each sublattice belong necessarily to the remaining $k-1$ sublattices. It can be easily shown that the stability regions for ordered states at temperature T in the system with a, b, and c interaction parameters are determined through the superposition (in chemical-potential–difference space) of the stability regions for uniform phases in a system described with fields given by

$$a'=-a,\quad b'=-b,\quad c'=-c,\quad T'=(k-1)^{-1}T\ , \quad (18a)$$

$$\nu_1'=\nu_1-q(k-1)^{-1}\left[b\sum_i z^{(i)}+c\sum_i y^{(i)}-a\sum_i y^{(i)}-b\sum_i x^{(i)}\right], \quad (18b)$$

$$\nu_2'=\nu_2-q(k-1)^{-1}\left[a\sum_i z^{(i)}+c\sum_i x^{(i)}-a\sum_i y^{(i)}-b\sum_i x^{(i)}\right]. \quad (18c)$$

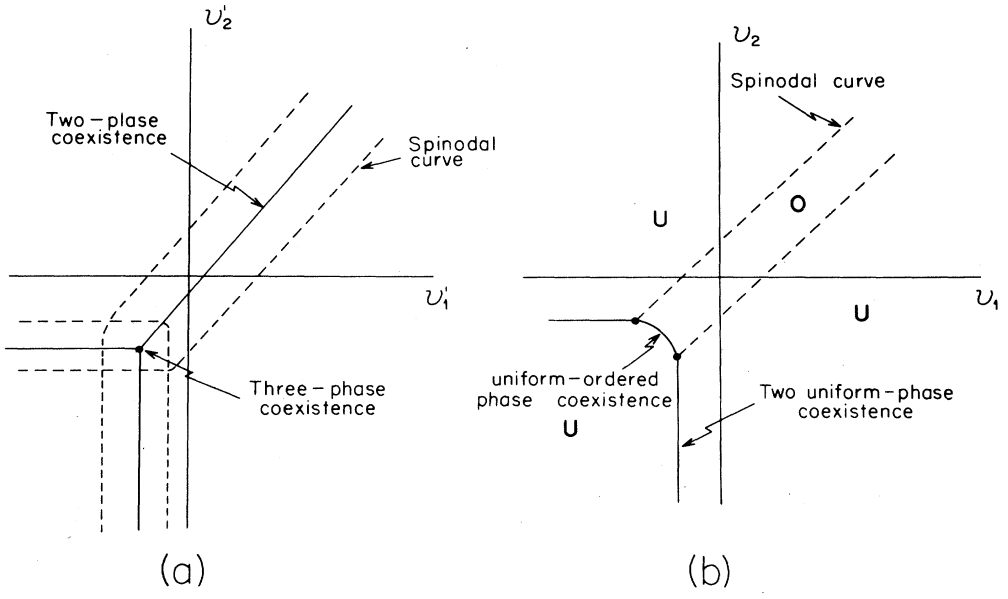

FIG. 3. (b) phase diagram that results after the transformation in Eqs. (14) is performed for the system in (a) and the stability of different resulting phases is analyzed.

There is another very useful mapping that relates the phase equilibrium properties between pairs of systems located along the symmetrical sections of the energy triangles. To describe this mapping, we first note from Eqs. (12) that for the systems located along $a=b$ the ordered states with symmetrically occupied sublattices $x^\alpha=y^\beta$ and $x^\beta=y^\alpha$ (with $z^\alpha=z^\beta$) require that $\nu_1=\nu_2$. We recall[1] too that phase coexistence between the uniform phases (x^α,y^β) and $(x^\beta=y^\alpha,y^\beta=x^\alpha)$ when $a=b$ also requires $\nu_1'=\nu_2'$. To determine the relationship between these states we substitute the sublattice-occupancies symmetry condition (along with $x+y+z=1$) into Eqs. (12) to obtain

$$\begin{aligned}\nu_1&=kT\ln(x^\alpha/z^\alpha)+q[b-2by^\alpha-(2b-c)x^\alpha]\\&=kT\ln(x^\beta/z^\beta)+q[b-2by^\beta-(2b-c)x^\beta]\,,\\\nu_2&=kT\ln(y^\alpha/z^\alpha)+q[b-2bx^\alpha-(2b-c)y^\alpha]\\&=kT\ln(y^\beta/z^\beta)+q[b-2bx^\beta-(2b-c)y^\beta]\,.\end{aligned}\tag{19}$$

These equations can be written in the form that Eqs. (4) take for the uniform states referred to above provided we adopt the particular transformation

$$\begin{aligned}&T'=T,\quad a'=b'=(2b-c)/2,\quad c'=-c\,,\\&\nu_1'=\nu_2'=\nu_1+qc/2\,.\end{aligned}\tag{20}$$

The transformation in Eqs. (20) above does not satisfy the normalization condition for the energy parameters in Eq. (5). An alternative formulation of this mapping that is compatible with this normalization condition is given by

$$T'=T/(|2a-c|-|c|)\,,\tag{21a}$$

$$c'=-cT'/T\,,\tag{21b}$$

and

$$a'=(2a-c)T'/(2T)\,.\tag{21c}$$

Employment of the symmetrical occupancies condition together with the transformation above into the expression for Π in Eq. (17) leads to the "pressure" equality $(\Pi')^\alpha=(\Pi')^\beta$ for phase coexistence between the two uniform phases α and β. Thus, this mapping reproduces all the phase-diagram features of the system $a'=b'$ in the diagram of the image system $a=b$. It can be concluded from the relations $2a'=2a-c$ and $c'=-c$, together with the normalization condition in Eq. (5), that intervals of the symmetrical sections of given length are imaged into intervals of different length. Thus, the images of the full $a=b$, $b=c$, and $c=a$ sections of the P triangle cover not only the same sections each in one of the adjacent Q triangles but also one-half in each of the $-a=-b$, $-b=-c$, and $-c=-a$ sections of the S triangle. In the same manner the other half of the symmetrical sections on triangle S are covered by the corresponding symmetrical section on triangles R. In Fig. 4 we show the value of the energy parameter c as the image system parameter c' is taken across the symmetric $a'=b'$ sections of the P and R triangles. The use of this mapping (along with the permutation properties of the triangles) makes it possible to obtain all system phase diagrams on the symmetrical sections of the eight energy triangles from the knowledge on the uniform-phase diagrams along the $a=b$ section of the P triangle and the sublattice-ordered phase diagrams along the $-a=-b$, $-c<\frac{1}{2}$ section of the S triangle. The first section is known from the work of FDG, while the second had to be explored by us via numerical calculations. These systems represent at least two interesting models: (i) binary alloys with one magnetic component and (ii) lattice models for micellar solutions. Since in the following two articles we discuss these two models in detail, our description here of the symmetric sections covers only some general features.

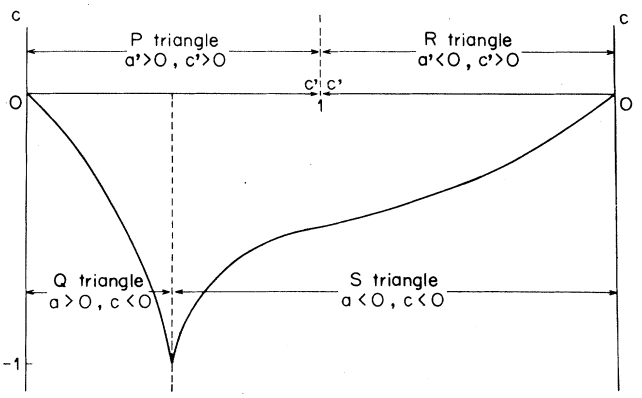

FIG. 4. Variation of energy parameter c with image parameter c' according to the transformation for symmetric sections in Eqs. (20).

III. THE GLOBAL PHASE DIAGRAM

A. General overview

The global phase diagram consists[1] of a set of manifolds or (hyper)surfaces (in the five-dimensional field space spanned by a, b, T, ζ_x, and ζ_y) that represent different kinds of phase coexistence and critical points. In the FDG work A^2 represents two coexisting phases and B denotes a conventional critical point where two phases coalesce. Likewise, three-phase states A^3 terminate at a critical end point AB or at a tricritical point C. Four phase states A^4 may appear bounded by critical points that coexist with two phases A^2B, by a double critical point B^2, by a tricritical end point AC, or by a fourth-order critical point D. Since according to the mapping in Eq. (14) every ordered state can be associated with two uniform-state free-energy minima, we extend the above notation to include sublattice-ordered phases in the following way. We represent a single ordered state by (AA), n-ordered phase coexistence by $(AA)^n$. Critical points arising from coalescence of only ordered phases are denoted by (BB), (CC), etc. The first, represents a critical point between two ordered states that results in an ordered state, while the second is a tricritical point between three ordered phases that become a single ordered state. Phase coexistence between n uniform and m ordered states is represented by $A^n(AA)^m$. A critical point where one ordered phase transforms into a uniform phase

is represented by (B). Coexistence between two ordered phases $(AA)^2$ may terminate following four different paths. (i) One state transforms into a uniform one in the presence of the other, this is denoted by $(B)(AA)$. (ii) The two ordered phases transform into a uniform phase simultaneously at a fourth-order critical point that we denote by $((D))$. (iii) The two phases simultaneously transform into two disordered phases at a critical point of the type $(B)^2$, which in turn may lead to phase coexistence A^2. And (iv) both phases become critical at the point labeled (BB), which can further transform into an ordered state (AA). Similarly, coexistence between one ordered state and a disordered one may evolve along the paths: $(AA)A \rightarrow (B)A \rightarrow A^2$ or $(AA)A \rightarrow (C) \rightarrow A$. The fourth-order multicritical point where two uniform and one ordered phases become identical is denoted by (D). The highest-order criticality observed in the sublattice divided model is a sixth-order multicritical point (F). This results from three- (ordered) phase coexistence terminating at a uniform state. This situation arises at four different isolated points in five-dimensional field space, whose projections fall, in energy space, at the center of the S triangle and at one point each on the symmetric sections of the R triangles. These and other kinds of manifolds appearing in the global phase diagram are listed in Table I.

In Fig. 2 we show the eight energy triangles with the 84 areas of distinct phase behavior. Of these, seventeen are qualitatively different and the rest may be constructed by symmetry. As in Ref. 1, each region in Fig. 2 is denoted by a capital letter that indicates the number of positive energy parameters ($P=3$, $Q=2$, $R=1$, $S=0$) followed by subindexes and occasionally by a prime. [To obtain the notation of sets of equivalent regions the subindexes α,β,γ must be permuted in the same manner as a,b,c (and x,y,z and ζ_x,ζ_y,ζ_z).] The systems that form the boundaries of the different two-dimensional regions have special properties, and the graphical representation we have chosen for these dividing lines in Fig. 2 is as follows. (i) Solid lines (other than sides of triangles) represent projections of C tricritical points in the case of the P triangle and (their continuations) on the adjacent triangles Q, and (C) tricritical points on triangle S and (their continuations) on triangles Q. Double solid lines on triangle S and on the adjacent triangles R represent systems for which both (CC) tricritical and $((D))$ fourth-order points occur. The dashed lines on triangles Q and R indicate the presence of fourth-order (D) points, and on triangle S the presence of fourth-order $((D))$ points. (ii) The dotted lines on the principal triangle P represent systems where four-uniform phase coexistence is possible in a finite range of temperatures (type-II A^4- states in the notation of Ref. 1). The same type of lines on triangles Q delimit zones where every system displays two distinct $A^2(AA)$

TABLE I. Notation for the different manifolds of the three-component model. Repeated letters within parentheses refer to ordered states. A letter within parentheses is used for those manifolds at which ordered states become uniform. Occasionally two parentheses are needed to distinguish between two different manifolds. Letters B $(=2)$ through F $(=6)$ denote the order of the critical point.

Manifold	Description
A^n	Coexistence of n uniform phases
B	Ordinary critical point between uniform phases
C	Tricritical point between uniform phases
BA	Critical end point among uniform phases
BA^2	Coexistence between two uniform phases and a critical state B
B^2	Double critical point between uniform phases
AC	Tricritical end point among uniform phases
D	Fourth-order multicritical point between four uniform phases
$(AA)^n$	Coexistence of n-ordered phases
(BB)	Critical point between two ordered states
$(BB)(AA)$	Critical end point among ordered phases
(CC)	Tricritical point between three ordered phases
$A^n(AA)^m$	Coexistence of n-uniform and m-ordered phases
$B(AA)$	Coexistence between an ordered phase and a critical state B
(B)	Critical state for an ordered phase transforming into a uniform phase
$A(B)$	Coexistence among a uniform phase and a critical state (B)
$A^2(B)$	Coexistence between a critical state (B) and two uniform phases
$(AA)(B)$	Phase coexistence between an ordered phase and a critical state (B)
$(B)^2$	Coexistence of two critical states (B)
$A(B)(AA)$	Coexistence among a uniform phase, a critical state (B), and an ordered phase (AA)
$(B)^2(AA)$	Coexistence between one ordered phase and a double critical state $(B)^2$
(C)	Tricritical point between a uniform state and an ordered phase.
$A(C)$	Coexistence between a uniform state and a tricritical (C) point
(D)	Fourth-order multicritical point among two uniform phases and one ordered phase
$((D))$	Fourth-order multicritical point between two critical ordered phases (BB)
(F)	Sixth-order multicritical point between three critical ordered states

states along a finite range of temperatures. On the S triangle these types of lines represent systems with a $(BB)(AA)$ point occurring at $T=0$, and delimit regions where $(AA)^3$ states occur. This is analogous to the case of systems located at the edges of the P triangle where BA points occur at $T=0$. (iii) The dashed-dotted lines on triangle S and adjacent triangles R delimit regions where there appear additional $A(AA)$-type states at intermediate temperatures. On triangles Q these lines separate systems differing in the high-temperature properties of their ordered states. (iv) The systems on the lines drawn with crosses on triangle S correspond to the symmetrical images of systems on triangle P that exhibit four phase coexistence of type II.

When the mappings described in Sec. III did not provide sufficient information we found it necessary to determine numerically the values of the parameters where the important features of the phase diagram occur. We give here the values for the location of some special points on the energy triangles. However, not all of the boundaries in Fig. 2 were determined with numerical precision, because the continuity in behavior associated with adjacent regions in energy space allowed us to complete the construction of the global phase diagram, with a fair degree of confidence, through consistency reasoning. There remains, of course, the possibility that we have overlooked some additional coexistence regions in the five-dimensional field space that our numerical work did not probe. Further numerical investigations would be required to rule out other kinds of behavior, or to confirm the assigned nature of the boundaries between different manifolds.

B. Triangle $a<0, b<0, c<0$

Within the S triangle (shown in detail in Fig. 5) it is possible to distinguish three qualitatively different kinds of system phase diagrams. These are shown in Figs. 6–8 and correspond, respectively, to the energy points labeled 1 to 3 in Fig. 5. In the central region of the triangle, the systems belonging to zones $S_{0\alpha}$, $S_{0\beta}$, and $S_{0\gamma}$ are characterized by three-phase equilibrium amongst ordered states. For every system in these regions the $(AA)^3$ lines extend from zero temperature to a critical end point $(BB)(AA)$. The three associated two-phase coexistence surfaces $(AA)^2$ are bounded at all temperatures by lines of critical points (BB). The stability regions for the ordered phases (O regions) are bounded at all temperatures by second-order transitions between ordered and uniform phases, i.e., lines of (B) critical points. The set of critical

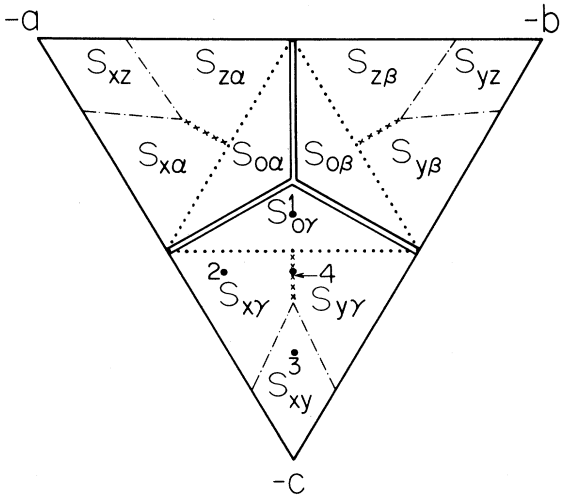

FIG. 5. Projection of the global phase diagram on the S energy triangle.

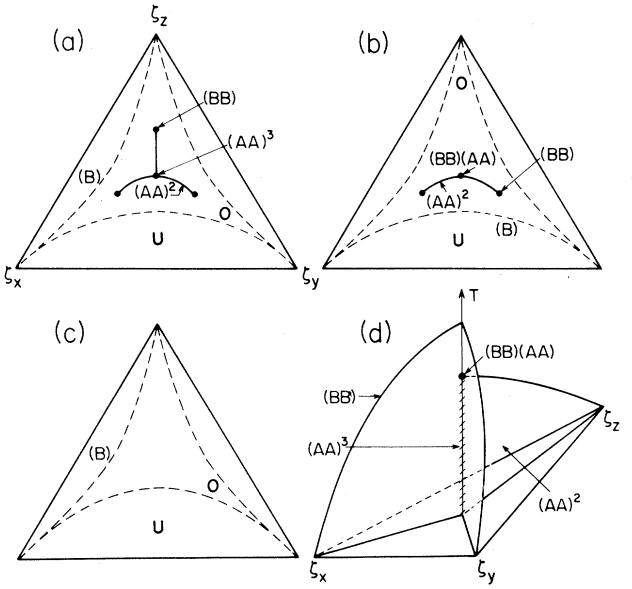

FIG. 6. System phase diagram for the energy point labeled 1 in Fig. 5 ($a=b=-0.3$ and $c=-0.4$). (a)–(c) show isothermal cuts at progressively higher temperatures, (d) shows ordered-phase coexistence surfaces. Similar sequences are shown for other energy points in the following figures.

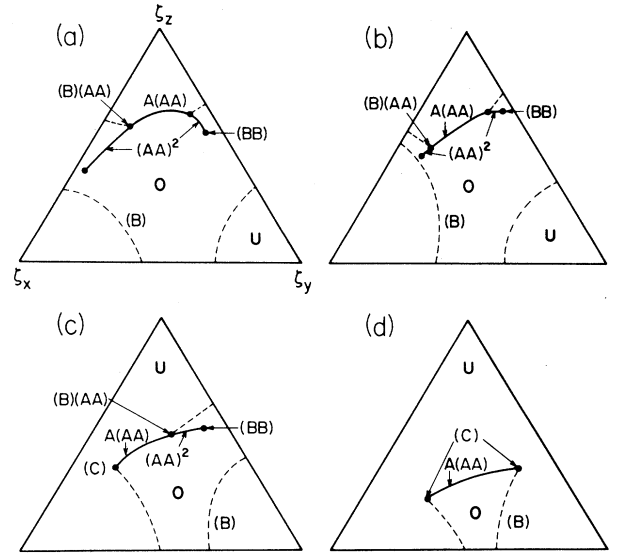

FIG. 7. System phase diagram for the energy point labeled 2 in Fig. 5 ($a=-0.2$, $b=-0.1$, and $c=-0.7$).

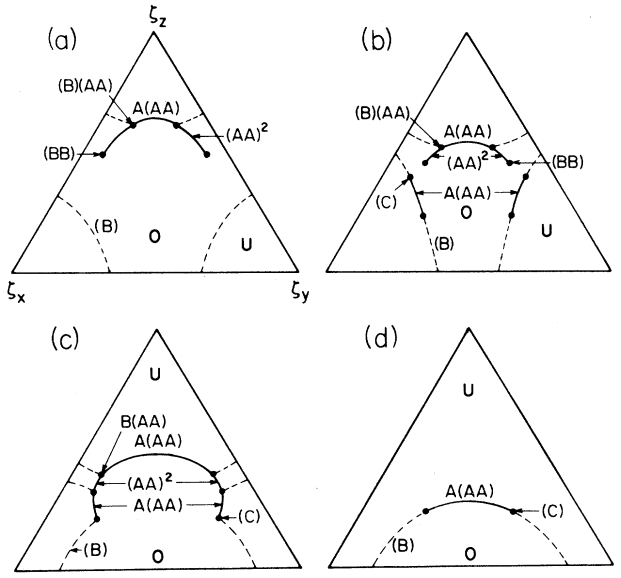

FIG. 8. System phase diagram for the energy point labeled 3 in Fig. 5 ($a=b=-0.1$ and $c=-0.8$).

(B) lines define a surface that extends from zero temperature and encloses the totality of the ordered states. A phase diagram characteristic of this region is shown in Fig. 6. Figures 6(a)–6(c) correspond to isothermal cuts at progressively higher temperatures. Figure 6(d) illustrates the ordered-states coexistence surfaces in field space.

The systems with energy points on the double solid lines in Fig. 5 that separate regions $S_{0\alpha}$, $S_{0\beta}$, and $S_{0\gamma}$ exhibit symmetrical phase diagrams with triple-point $(AA)^3$ lines that terminate at a tricritical point (CC), the common end of three critical (BB) lines. These double solid lines, the projection of the (CC) points, originate at the center of the S triangle and terminate in the adjacent R triangles. The center of the S triangle, the rear-shield region, represents a system with a multicritical point (F) where not only do the three ordered phases become identical but they also transform into a uniform phase. There, the common end of the three critical (BB) lines touches one branch of the critical (B) surface. The three tricritical (CC) lines (in the five-dimensional field space) simply converge into a single higher-order critical point (F). This connectivity of tricritical lines coincides with that suggested in Ref. 1 as a possible alternative to the topology of the shield region at the center of the triangle P.

If we now move the energy point from the center of the S triangle towards any of the dotted lines in Fig. 5, the critical end point (BB)(AA) [see Fig. 6(d)] shifts to lower temperatures, reducing the span of the three-phase points $(AA)^3$ until they disappear when the point (BB)(AA) reaches $T=0$ at the dotted lines. In Fig. 7 we show a phase diagram representative of a system located in the region labeled $S_{x\gamma}$. This type of system presents a two-phase coexistence surface of the type $A(AA)$ that arises from zero temperature. This surface is also bounded by two lines of (B)(AA) end points and continues into the ordered-states phase region as two wings of $(AA)^2$ coexistence sheets. At higher temperatures, the two lines of (BB) critical points, that border the coexistence wings $(AA)^2$, intersect the critical surfaces (B) at two tricritical points of the type (C). Above these temperatures only the $A(AA)$ coexistence surface remains.

If we move now the energy point from region $S_{x\gamma}$ to region S_{xy} in Fig. 5 two additional equilibrium surfaces of $A(AA)$ type appear within a finite range of temperatures, so that at these temperatures there are three branches of $A(AA)$-type coexistence [see Fig. 8(b)]. At higher temperatures the (BB) lines that border the $(AA)^2$ wings intersect one of the two (C) lines that limit the $A(AA)$ surfaces originating a new (B)(AA) line from a ((D)) state [see Fig. 8(c)]. The $(AA)^2$-type coexistence disappears along with the two lateral branches of O regions [Figs. 8(c)–8(d)] leaving only an $A(AA)$ coexistence surface, which is limited by a line of critical points (C), and disappears when the temperature is further raised.[3] As we move within zone S_{xy} towards that part of the symmetrical section of triangle S marked by a line of crosses in Fig. 5, the two wings of $A(AA)$ coexistence reduce in extent on approaching the dashed-dotted lines where they disappear. At the same time the high-temperature central surface of $A(AA)$ coexistence bounded by (C) lines shrinks.

A representative phase diagram for the symmetrical systems on the line of crosses in Fig. 5 is shown in Fig. 9. A low-temperature isothermal cut is shown in Fig. 9(a), where the interesting feature is a line of two-phase coexistence $A(AA)$ points. This arises from zero temperature and is bounded by two different (B)(AA) critical points, the result of the intersection of the $(AA)^2$ and the (B) coexistence surfaces. The two branches of $(AA)^2$ points are in turn bounded by (BB) critical lines. If temperature is increased, see Figs. 9(b)–9(d), $A(AA)$-type

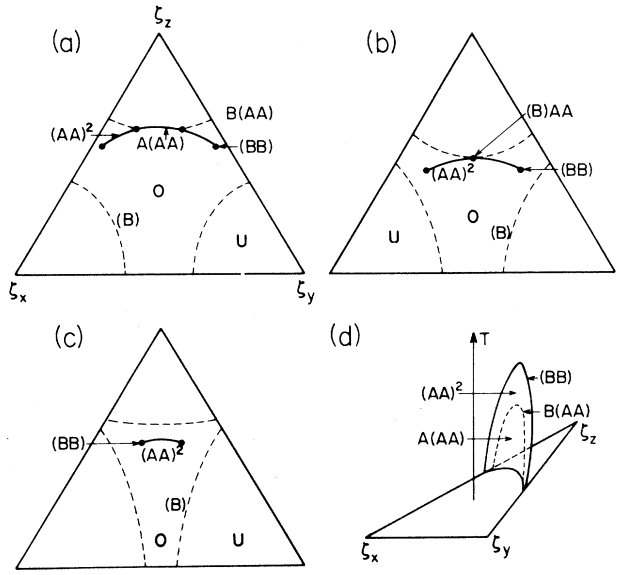

FIG. 9. System phase diagram for the energy point labeled 4 in Fig. 5 ($a=b=-0.2$ and $c=-0.6$).

coexistence disappears through the merging of the two lines of $(B)(AA)$ points leaving a single $(AA)^2$ surface [Fig. 9(c)]. See Fig. 9(e) for a representation in field space. The symmetrical section for this type of system is bounded by the energy point $(-0.186,-0.186,-0.628)$ which is the image (under the mapping for symmetrical sections) of the ferromagnetic D_c fourth-order point of Ref. 1. The D_c point marks the beginning of the type-II $(A^4)_c$ coexistence region on triangle P. Under the mapping for the symmetrical sections, $A(AA)$ coexistence corresponds to uniform-states three-phase coexistence, the symmetrical $(B)(AA)$ point corresponds to the lower critical end points $(BA^2)_c$, coexistence of two ordered states to four-phase coexistence $(A^4)_c$ and the symmetrical (BB) critical points to the $(B^2)_c$ double critical points in the notation of FDG. This behavior terminates at the energy point $(-\frac{1}{4},-\frac{1}{4},-\frac{1}{2})$, image of the (0,0,1) point of the P triangle.

C. Triangle $a<0$, $b<0$, $c>0$

We now describe the system phase diagrams belonging to R-type triangles. In Fig. 10 we show the R triangle for which the parameter c is positive, and in Figs. 11–13 we show the phase diagrams that correspond to the energy points labeled 5–7, respectively, in Fig. 10. Since now c is positive, uniform two-phase coexistence of the A^2 type must be present at low temperatures for all energy points. At fixed temperature this line emerges from the $\zeta_z=0$ activity axis that represents $(x,y,z=0)$ binary mixtures. Energy points on region $R_{\alpha\beta}$ generate phase diagrams similar to those described before for the S_{xy}-type region. The main difference between the S_{xy} and the $R_{\alpha\beta}$ system phase diagrams is the continuation of the low-temperature $A(AA)$-coexistence surface of the S_{xy}-type diagrams into a uniform two-phase coexistence A^2 surface. This occurs because one of the three O regions present on the S triangles does not form in the $R_{\alpha\beta}$ systems. The A^2 surface is bounded by a line of ordinary critical points B and by the $A(B)$ coexistence line. At in-

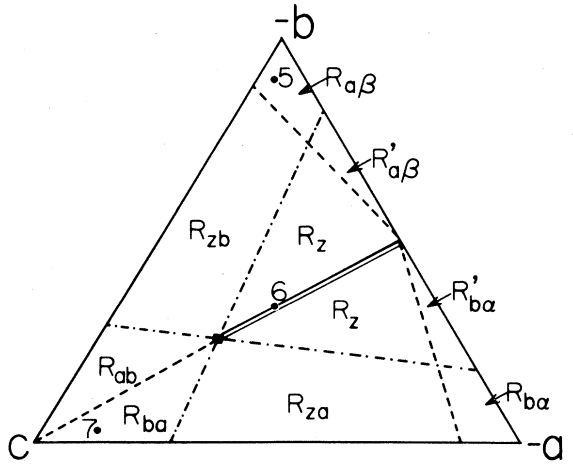

FIG. 10. Projection of the global phase diagram showing the R energy triangle with $a<0$, $b<0$, $c>0$.

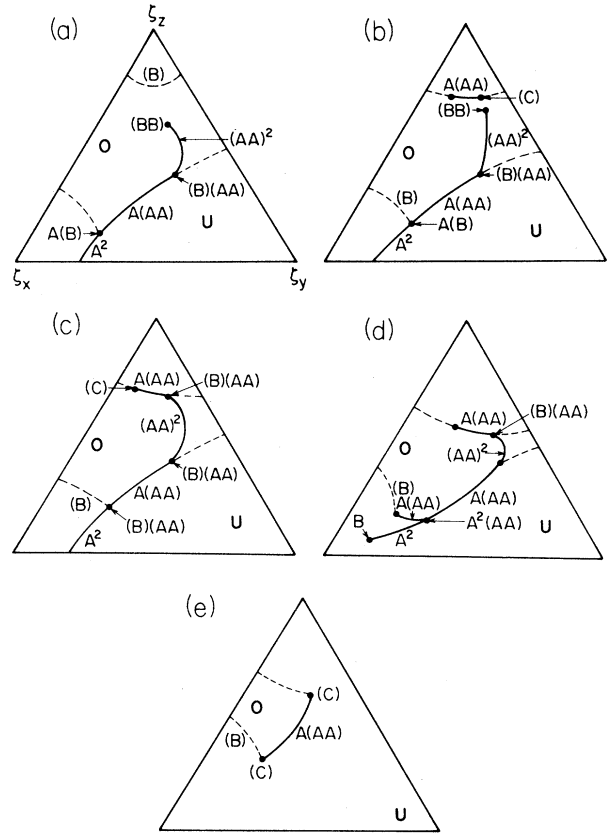

FIG. 11. System phase diagram for the energy point labeled 5 in Fig. 10 ($a=-0.05$, $b=-0.9$, and $c=0.05$).

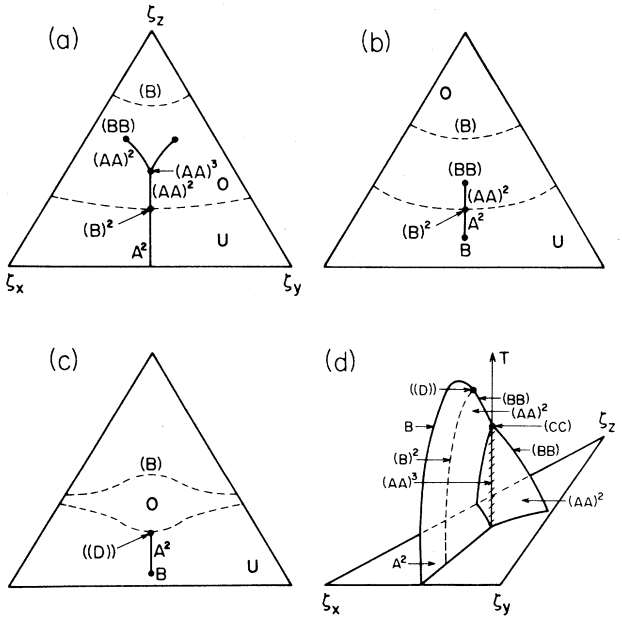

FIG. 12. System phase diagram for the energy point labeled 6 in Fig. 10 ($a=b=-c=-\frac{1}{3}$).

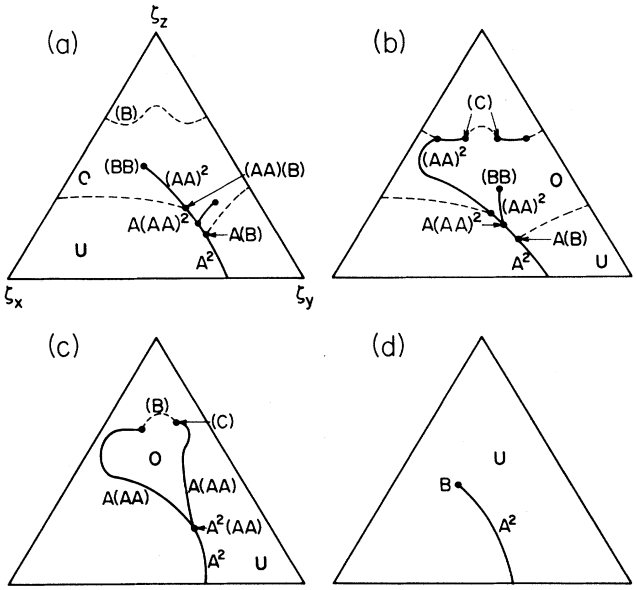

FIG. 13. System phase diagram for the energy point labeled 7 in Fig. 10 ($a=-0.013$, $b=-0.07$, $c=0.8$).

termediate temperatures two new $A(AA)$-coexistence surfaces emerge, one of them develops from the $A(B)$ line and generates a line of three-phase coexistence of the type $A^2(AA)$ [see Fig. 11(d)] which is bounded by $A(B)$ and $B(AA)$ critical points at low and high temperatures, respectively. The manifolds of type $A^2(AA)$ are similar to those found by FDG for the uniform model in this energy-space region except that here one of the states involved in the three-phase coexistence falls within the O-region. Because the energy point representative of this region, labeled 5 in Fig. 10, satisfies $|a|<|b|$, the zone of ordered states that emerges from the $\zeta_x=0$ activity-triangle side terminates at lower temperature than that originating at the $\zeta_y=0$ side. This development brings along the shrinking and vanishing of the $(AA)^2$ surface as temperature is raised. The prevalence of uniform A^2 phase coexistence over $A(AA)$ equilibrium rules out the appearance of more than one equilibrium zone $(AA)^2$. The system phase diagrams on region $R'_{\alpha\beta}$ differ from those for region $R_{\alpha\beta}$ in that one of the $A(AA)$ wings for intermediate temperatures is absent. When the energy point approaches the dashed lines on Fig. 10 the points $B(AA)$ and $A(B)$ that bound the $A^2(AA)$ three-phase coexistence line in the $R_{\alpha\beta}$-type diagrams come closer together. On the dashed line they meet at a critical point (D), and, as a consequence of this, the regions of the type R_{zb} and R_z no longer exhibit $A^2(AA)$ coexistence. Phase diagrams in these regions are similar to those found in regions $R_{\alpha\beta}$ and $R'_{\alpha\beta}$ in all other respects.

In the symmetric section of this triangle we find a special point, denoted by a solid square on Fig. 10, at which the double solid line [projections of both $((D))$ and (CC) points] that originated at the S triangle transforms into the dashed line [projections of (D) and $(B)^2(AA)$ points]. This point is located at $a=-\frac{1}{4}$, $b=-\frac{1}{4}$, and $c=\frac{1}{2}$ (and its permutations give the positions of two additional and equivalent points on the other two R triangles). In Fig. 12 we show several isothermal cuts of the phase diagram corresponding to point 6 on Fig. 10 on the double solid line. The first-order A^2 transitions between uniform states transform into $(AA)^2$ states when the O-region stability zone is entered; this occurs via a $(B)^2$ point. In the interior of the O region an $(AA)^3$ line connects this $(AA)^2$ manifold with other two $(AA)^2$ surfaces, each bounded by a line of (BB) points. At higher temperatures the triple line terminates at a (CC) point, the intersection of three (BB) critical point lines, two approaching from low temperature and the other from high temperature. The remaining high-temperature $(AA)^2$ coexistence ends at a $((D))$ fourth-order point arising when the (BB) and the $(B)^2$ lines touch. In Fig. 12(d) we show this behavior in $(\zeta_x,\zeta_y,\zeta_z,T)$ space. There, we show only the cut of the (B) surfaces within the A^2 coexistence surface, i.e., the $(B)^2$ points. The energy point denoted by the solid square in Fig. 10, is the image point of the center of the rear-shield region under the transformation in Eqs. (20) (see Fig. 4), and therefore it is also a sixth-order critical point (F). There, the triple line $(AA)^3$ terminates; also there the surface of (B) critical points that envelopes the ordered states touches both the B line of A^2 uniform phase coexistence and the (BB) line that bounds the low-temperature wings of $(AA)^2$ ordered phase coexistence. That is, there the (CC) and $((D))$ lines in five-dimensional space merge.

At the other side of this point, $(c>\frac{1}{2})$ in the symmetric zone between regions of the type R_{ab} and R_{ba}, the three-phase coexistence states $(AA)^3$ exist at low temperatures. The symmetric branch of $(AA)^2$ coexistence arises from the A^2-coexistence surface found by FDG for these energy points as it touches the (B) boundary of ordered-states stability regions. As temperature is raised the $(AA)^2$ states come closer to the (B) boundary and generate a point of the type $(B)^2(AA)$ when these two types of states touch. At higher temperatures two new branches of $A(AA)$ coexistence originate at the high-ζ_z boundary of the O region. These two branches merge with the remaining nonsymmetrical branches of $A(AA)$ coexistence generating a loop that encloses the O region. This loop shrinks with increasing temperature and collapses at a (D) multicritical point. Close to these symmetric points, in regions of the type R_{ab}, the coexistence zones are not symmetrical. This causes an intersection at nonsymmetric locations between the (B) surfaces and the branch of phase segregation originating at $\zeta_z=0$. As a consequence of this $A(AA)^2$ transitions are observed at low temperatures [see Fig. 13(a)]. At intermediate temperatures, two new branches of $A(AA)$ coexistence appear at the high ζ_z boundary of the O region. These grow and merge with the two critical points (BB) when the ordered-state stability zone detaches itself from one of the edges of the activity triangle, then a loop bounds the O region [see Fig. 13(c)]. At these temperatures, and on the other side of the activity triangle, the line of $A(AA)^2$ states crosses the (B) surface at a $A(B)(AA)$ coexistence point from which a line of $A^2(AA)$ points continues and terminates at a point $A(C)$. This very complicated be-

havior disappears at zero temperature at the boundaries between the R and the Q triangles.

D. Triangle $a>0, b>0, c<0$

The Q triangles are characterized by the presence of two well-defined surfaces of uniform-states phase equilibria, which restrict further the zones for stable ordered states. As shown in Fig. 14, we distinguish in these triangles six zones of distinct phase behavior. In zones $Q'_{b\gamma}$ we find a surface of uniform A^2 transitions that extend from the pure binary limits, $\zeta_x=0$ (the $x=0$ binary alloy) and $\zeta_y=0$ (the $y=0$ binary alloy). This surface intersects the spinodal surface (B) for ordered-states stability at two critical points of the type $A(B)$. Between these two points, the first-order transitions A^2, transform into those of the type $A(AA)$. At higher temperatures, the triple line of A^3 phase coexistence found in the ferromagnetic study of FDG (Ref. 1) appears here transformed into a three-phase coexistence of the type $A^2(AA)$ [Fig. 15(b)]. This line[1] does not extend to zero temperatures, and is bounded by an $A(B)$ point from below and a $B(AA)$ point from above. Phase coexistence of the type $A(AA)$ disappears when the two (B) surfaces that comprise the regions of ordered states merge and detach from the segregating branch, as shown in Fig. 15(d). Phase diagrams in regions denoted by Q_{ab} in Fig. 14 represent a superposition of the triple lines and corresponding critical end points from the phase diagrams in regions $Q'_{b\gamma}$ and $Q'_{a\gamma}$. As in the case of FDG the triple lines do not meet in the full five-dimensional field space. Again the only difference between our results and those of FDG originates from the intersection of the (B) surfaces with the A^2 surfaces, generating, in this case, two triple lines of the type $A^2(AA)$.

Close to the other corners of triangle Q, in regions labeled $Q_{b\gamma}$ and $Q_{a\gamma}$ (point 9 in Fig. 14), the ordering tendency is less pronounced, as this is determined by the value of the energy parameter c, and the ordered-states stability region does not mask uniform A^3 triple lines. It

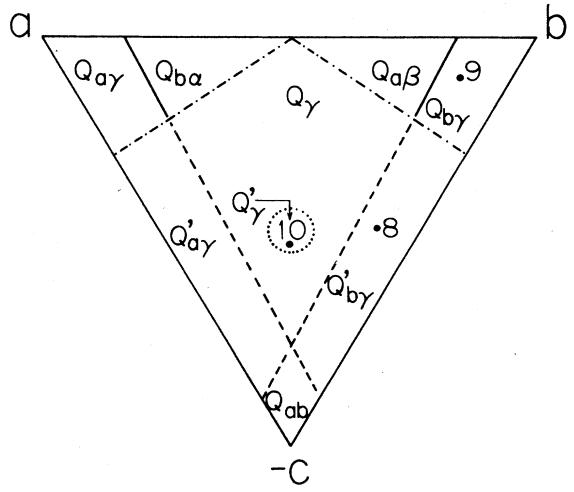

FIG. 14. Projection of the global phase diagram showing the Q energy triangle with $a>0, b>0, c<0$.

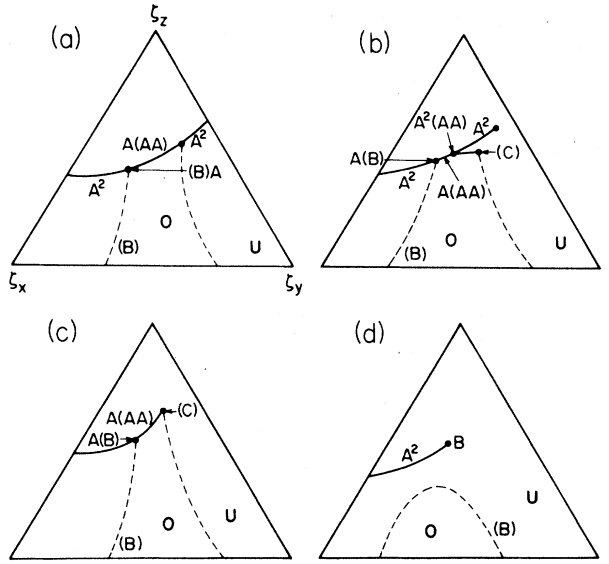

FIG. 15. System phase diagram for the energy point labeled 8 in Fig. 14 ($a=0.1, b=0.45, c=-0.45$).

is clear from Fig. 16 that the evolution of the triple lines is completely equivalent to that obtained by FDG in the same regions and these manifolds appear bounded by BA critical end points at high and low temperatures. The dashed and solid lines in Fig. 14, represent the end of regions with three-phase manifolds. In the case of the boundaries between regions $Q_{b\gamma}$ and $Q_{a\beta}$, the solid lines in Fig. 14 represent manifolds of tricritical C points, while in the case of the boundaries between regions $Q'_{b\gamma}$ and Q_{γ} (or Q_{ab}) they represent (D) fourth-order critical points. There are no three-phase manifolds in regions

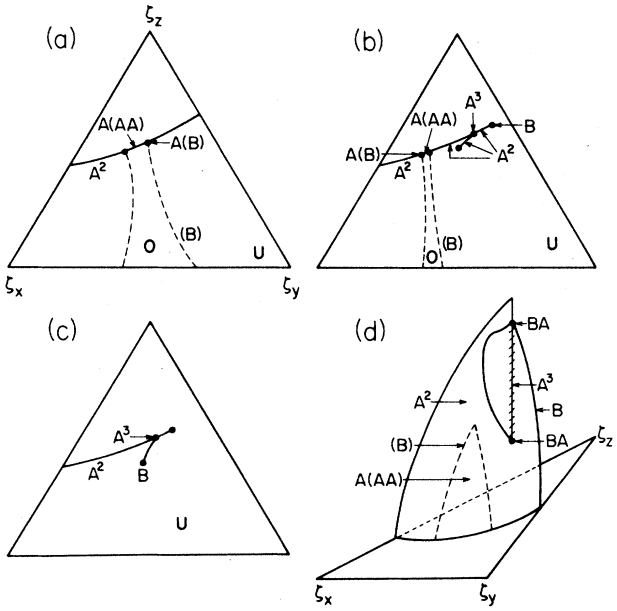

FIG. 16. System phase diagram for the energy point labeled 9 in Fig. 14 ($a=0.1, b=0.8, c=-0.1$).

$Q_{a\beta}$ ($Q_{b\alpha}$) and Q_γ. Their phase diagrams are similar to those obtained for their neighboring regions in all other respects. Dashed-dotted lines between $Q_{a\beta}$ ($Q_{b\alpha}$) and Q_γ differentiate zones where the O region collapses ($Q_{a\beta}$ and $Q_{b\alpha}$) from that where the O-region persists.[3]

The symmetric transformation described in the Sec. II maps the central point of the shield region on triangle P into the point ($a=\frac{1}{4}$, $b=\frac{1}{4}$, $c=-\frac{1}{2}$) marked by a dot in Fig. 14. The image of the shield region on the symmetrical section in this Q triangle is bounded by the points ($a=0.292$, $b=0.292$, $c=-0.416$) and ($a=0.236$, $b=0.236$, $c=-0.529$). We have denoted this region by Q'_γ and isothermal cuts of a representative system phase diagram are shown in Fig. 17.[3] On the symmetric sections of these uniform diagrams ($\zeta_x=\zeta_y$), we can recognize the familiar structure of the phase diagrams of the shield region. The coexistence line between ordered and uniform phases $A(AA)$ that originates from zero temperature is the image of the symmetric A^3 line on the P triangle [Figs. 17(a) and 17(b)], the four-phase coexistence points that form a continuous manifold in the five-dimensional field space in the shield region of the P triangle, now appear as coexistence lines of the type $A^2(AA)$. As shown in Figs. 17(b) and 17(c), these $A^2(AA)$ points join the symmetric three-phase coexistence line with another two (asymmetric) lines of three-phase coexistence, and also with two uniform A^2 lines. At higher temperatures, the branch of A^2 transitions detaches from the $A(AA)$ transition, and the ordered-states stability region finally closes into the image line of the C_c manifold in FDG [which here represents the manifold of (C) points]. This interpretation (provided by our two mappings) clearly indicates that the boundaries of the Q'_γ region along the symmetrical section of the triangle Q correspond to $(C)A$ states ($c=-0.416$) and $B(AA)$ states ($c=-0.529$), images of the CA and BA^2 points, respectively, that bound the symmetrical section of the shield region of triangle P.

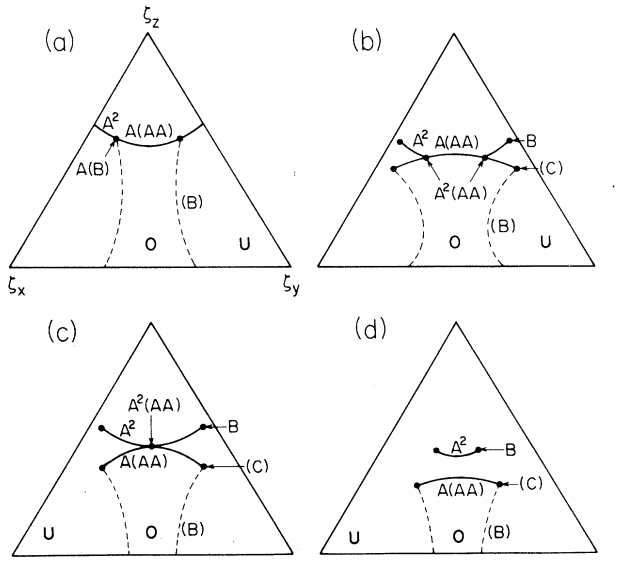

FIG. 17. System phase diagram for the energy point labeled 10 in Fig. 14 ($a=b=\frac{1}{4}$, $c=-\frac{1}{2}$).

E. Triangle $a>0$, $b>0$, $c>0$

If an energy point in regions $Q_{a\beta}$ or $Q_{b\gamma}$ is moved into the principal energy triangle P (shown in detail in Fig. 18), the ordered-states stability region shown in Fig. 16 is still found in the regions comprised between the edges of the P triangle and the dotted circle in Fig. 18. The O regions appear now reduced in extent in the activity triangle and they no longer touch its sides. As it turns out, these ordered states are always metastable or unstable with respect to uniform states and therefore, the global phase diagram associated with this region excludes the possibility of phase equilibrium between uniform and ordered phases. Its general behavior is that described in detail by FDG.

IV. DISCUSSION

We have explored the phase behavior of the FDG three-component model when a two interwoven sublattice subdivision is considered. We have combined our findings into a global phase diagram that comprises all of the eight interaction-energy–parameter triangles. The antiferromagnetic phase behavior found was compared with, and superposed on, the original ferromagnetic phase diagram of FDG.[1] Our main results are the following. There is a competition between ordering and segregation modulated by the values of the energy parameters a, b, and c. When they are all positive, on the principal triangle, only uniform phases are equilibrium states, even metastable ordered phases can occur only outside the circle marked in Fig. 18. All the features obtained by FDG (Ref. 1) for this triangle are preserved under sublattice subdivision, such as the shield region, the D points and

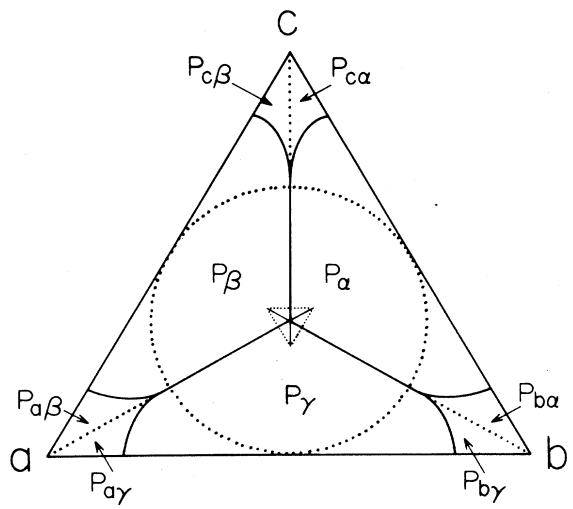

FIG. 18. Projection of the global phase diagram showing the P energy triangle. Metastable ordered states only occur outside the dotted circle.

the C lines. On the other hand, when all the energy parameters are negative, on the S triangle, the opposite situation prevails and equilibrium uniform states can only occur by themselves or coexist with ordered states. Ordered states are common on this triangle and become associated with lines of (CC) tricritical points that stem from a sixth-order multicritical point (F) at the center of the triangle. Also, other, (C)-type, tricritical points are often found on this triangle. On triangles Q and R an intermediate situation arises, and a portion of the uniform-phase features described by FDG becomes metastable with respect to ordered-phase states, more so on the R triangles than on the Q triangles. A rich collection of multicritical points and lines was found on these six triangles and include three sixth-order (F) states, lines of fourth-order $((D))$, and (D) points and tricritical (C) points. The two mappings between uniform- and ordered-phase properties for pairs of energy points described in Sec. II provide an understanding of how all of these features of the global phase diagram are interrelated.

A predominant characteristic of the phase diagram of the sublattice-divided model is the (B)-critical hypersurface that bounds the stability region for the ordered states. The nature of this hypersurface is intimately related to the particular lattice and sublattice subdivision chosen. There are lattices, like the fcc lattice, such that nearest-neighbor sites may belong to the same sublattice under two-sublattice subdivision. In this case order-disorder transitions are of the first order except at a few points in field space. This situation is similar to the case of solid-liquid transitions where critical melting can occur only at isolated points.

The system phase diagrams associated with the symmetrical sections of the energy triangles, that as we have seen display most of the highest-order critical states found, are usually the sections of interest in applications such as magnets and alloys,[1] and micellar solutions.[5] In the following two papers we review the properties of these sections in the languages of binary alloys with one magnetic component and of a model binary mixture of amphiphiles in a solvent. There we appreciate how the competition between ordering and segregation referred to above describes the transit from segregation and ferromagnetic to ordering and antiferromagnetic alloys, or from uniform solvent-amphiphile solutions to liquid-crystalline–type phases.

As pointed out in the work of FDG we do not expect that all descriptions of real systems are appropriately obtained by fixing a point in energy-parameter space. Instead, some descriptions may require a movable point (a,b,c) whose position depends on the temperature and the chemical potentials. Lattice models for microemulsions equivalent to the FDG three-component model with field-dependent energy points have been proposed and their properties studied.[6]

ACKNOWLEDGMENTS

This work was supported in part by Consejo Nacional de Ciencia y Tecnología (CONACyT) de México.

[1]D. Furman, S. Dattagupta, and R. B. Griffiths, Phys. Rev. B **15**, 441 (1977). Earlier work on the spin-1 model is well documented in this paper.

[2]R. L. Scott and P. H. van Konynenburg, Dicuss. Faraday Soc. **49**, 87 (1970); R. L. Scott and Ber Bunsenges, Phys. Chem. **76**, 296 (1972); P. H. van Konynenburg and R. L. Scott, Philos. Trans. Soc. London, Ser. A **298**, 495 (1980); see also D. Furman and R. B. Griffiths, Phys. Rev. A **17**, 1139 (1978).

[3]Y. Saito, J. Chem. Phys. **74**, 713 (1981).

[4]D. A. Lavis and G. M. Bell, Philos. Mag. **15**, 587 (1967).

[5]A. Robledo, Phys. Rev. A **36**, 4067 (1987).

[6]C. Varea and A. Robledo, Phys. Rev. A **33**, 2760 (1986); A. Robledo, Eurphys. Lett. **1**, 301 (1986); *Statistical Mechanical Models for Micellar Solutions and Microemulsions,* Proceedings of the 4th Mexican School on Statistical Physics, Oaxtepee, 1987, edited by C. Varea and R. Peralta (World Scientific, Singapore, 1988).